Available online at www.sciencedirect.com

SciVerse ScienceDirect

Ceramics International 39 (2013) 8549–8553

CERAMICS INTERNATIONAL

www.elsevier.com/locate/ceramint

Short communication

The influence of particle in-flight properties on the microstructure of coatings deposited by the supersonic atmospheric plasma spraying

Y. Bai[a,b], K. Liu[a], Z.H. Wen[c], J.J. Tang[a], L. Zhao[a], Z.H. Han[a,*]

[a]State Key Laboratory for Mechanical Behavior of Materials, Xi'an Jiaotong University, Xi'an 710049, China
[b]School of Mechanical Engineering, Xi'an Jiaotong University, Xi'an 710049, China
[c]Materials Science and Engineering School, Nanchang Hangkong University, Nanchang 330034, China

Received 9 February 2013; received in revised form 20 March 2013; accepted 29 March 2013
Available online 9 April 2013

Abstract

In this work, yttria-stabilised zirconia (YSZ) coatings were deposited by a high-efficiency supersonic atmospheric plasma spraying (SAPS) system. During spraying, the in-flight properties (including velocity and surface temperature) of the sprayed particles were diagnosed on-line by a commercially available Spray Watch 2i system positioned normal to the spraying axis. The effect of the in-flight properties of the sprayed particles on the microstructure of the coatings was studied, with the aim of achieving improved knowledge on the accurate control of their coating quality. The *VT* value, defined as a function of the in-flight velocity of the particles and the surface temperature of the substrate, was observed to be directly proportional to the reciprocal of the porosity and structure uniformity of the coatings, which indicated that the structure of the SAPS-coatings can be tailored by adjusting the *VT* value of the sprayed particles.

Keywords: Supersonic atmospheric plasma spraying; In-flight particle; Velocity; Surface temperature

1. Introduction

Plasma spraying is a powerful materials processing technique for depositing various functional coatings, especially some important anti-wear, corrosion resistant and thermal barrier coatings [1,2]. The microstructure of a plasma-sprayed coating is greatly influenced by the deformation behaviour of the particles impinging onto the substrate and by the characteristics of the underlying surface [3–6]. Experimental and theoretical evidence suggests that the spreading and cooling of molten particles on the surface depends on the following: (1) the particle size, velocity, and molten state prior to impact; and (2) the substrate roughness, temperature, and surface reactivity [7,8]. To date, the microstructures of plasma-sprayed coatings are often optimised and tailored by empirically tuning a large number of process parameters, followed by examination of the coatings by metallographic observation. This complicated and time-consuming optimisation method requires control over 35 main macroscopic parameters [9]. In addition, some other factors, such as electrode erosion and fluctuations of the powder injection geometry, are uncontrollable [10]. Thus, it is a significant challenge for scientists and engineers to accurately control the microstructure of an as-sprayed coating during the plasma spraying process. Some studies have suggested that the velocity and temperature of each in-flight particle are two of the primary parameters influencing the microstructure of coatings because they dramatically influence the flattening behaviour of the particles and ultimately the microstructure of the coating [11,12].

Recently, an advanced high-efficiency supersonic plasma spraying system (SAPS) was successfully developed by the National Key Laboratory for Remanufacturing (Beijing, China) for the deposition of ceramic and metallic coatings with good performance [13–15]. Our previous results demonstrated that the SAPS-coatings exhibited a finer microstructure and higher bonding strength than the coatings deposited by conventional atmospheric plasma spraying [16]. The SAPS method is primarily used to deposit high-performance ceramic coatings at low cost. However, little information is available on the effect of the in-

*Corresponding author. Tel.: +86 2982668614; fax: +86 29 82663453.
E-mail address: zhhan1955@163.com (Z.H. Han).

0272-8842/$ - see front matter © 2013 Elsevier Ltd and Techna Group S.r.l. All rights reserved.
http://dx.doi.org/10.1016/j.ceramint.2013.03.091

flight properties of the sprayed particles on the microstructure of the SAPS-coatings. Therefore, the deposition of yttria-stabilised zirconia (YSZ) coatings using a high-efficiency supersonic atmospheric plasma spraying (SAPS) system was studied in this work. The influence of the in-flight properties of the sprayed particles on the microstructure of the resulting coatings was studied, with the goal of achieving improved knowledge of the accurate control of the coating quality.

2. Experimental procedure

The substrate, GH3030 nickel-based superalloy with dimensions of 35 mm × 14 mm × 3 mm, was ultrasonically cleaned and subsequently grit-blasted with alumina powder. The surface roughness (R_a) of the grit-blasted substrate was 6.3 ± 0.4 μm, as measured with a profilometer (TR 240, Beijing Time Group, Beijing, China). The spray-dried and sintered ZrO_2–8 wt% Y_2O_3 (YSZ) powders with particle sizes in the range of 25–90 μm were used as the feedstock to deposit coatings using the SAPS system. The spray parameters are presented in Table 1. During spraying, a commercially available Spray Watch 2i system (Osier, Finland) was used to monitor the velocity and surface temperature of the in-flight particles. The substrate was cooled by compressed air, and the temperature of the substrate was held at 150 ± 30 °C, as monitored by a NiCr/NiSi thermocouple attached to the back of the substrate. The porosity of the coatings was estimated by quantitative image analysis (IA) using a picture analysis system of magnified images obtained by scanning electron microscopy (SEM; VEGAII XMU, Tescan, Czech Republic). In the image analysis, a series of SEM images with 1000 × magnification were obtained for individual specimens to obtain a representative porosity value. The image resolution was 600 dpi, and the minimum area of the detectable voids was approximately 0.1 μm^2. Twenty SEM micrographs of the cross section of each coating were randomly selected. The coating microhardness was measured with a microhardness tester (Micro Met 3 microhardness tester, Buehler Ltd., USA). The polished cross section of the coating was measured 20 times at different areas with a load of 2.94 N and a holding time of 10 s. The microhardness data scatter was processed using the Weibull statistical analysis [17,18].

Table 1
Spray parameters for YSZ powders.

Parameters	Value
Current (A)	400
Voltage (V)	160
Primary gas Ar (slpm)	60
Second gas H_2 (slpm)	17
Carrier argon gas flow rate (slpm)	7.5
Powder feed rate (g/min)	40
Spray distance (mm)	80, 100,120, 140

3. Results and discussion

Fig. 1 shows the cross-sectional SEM images of YSZ coatings deposited at the four distances of 80 mm, 100 mm, 120 mm and 140 mm. As shown in Fig. 1(a), many coarse cracks and pores were observed in the coating deposited at 80 mm. At the higher spray distance of 100 mm (as shown in

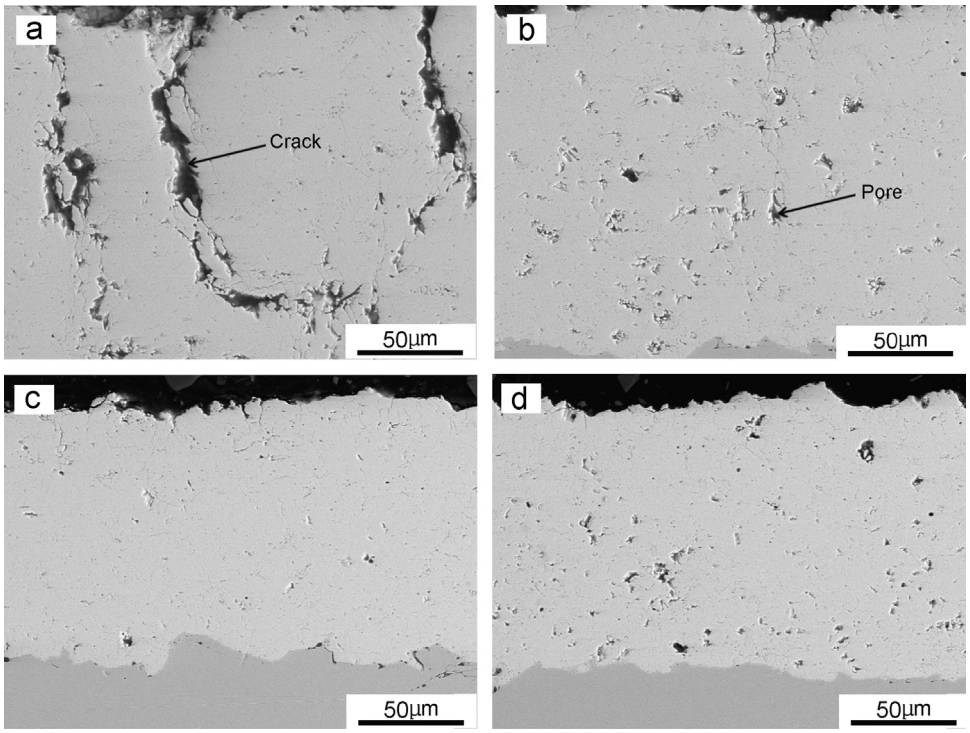

Fig. 1. Cross-sectional SEM images of coatings deposited at different spray distances: (a) 80 mm, (b) 100 mm, (c) 120 mm, and (d) 140 mm.

Fig. 1b), these coarse cracks were not observed in the sprayed coating, but some pores were still observed. However, as seen in Fig. 1(c), the coating was almost completely dense when the spray distance was 120 mm. For the highest spray distance studied of 140 mm, as seen in Fig. 1(d), the number of pores increased compared with the coating prepared at 120 mm. The porosities of the four coatings determined by image analysis were approximately 10%, 3%, lower than 1% and 3%. Fig. 2 shows the probability function of the Weibull plots of the Vickers hardness of the four coatings. As shown in Fig. 2, the Vickers hardness of the four coatings exhibited some scatter due to the non-uniform microstructure of the as-sprayed coatings. The Weibull modulus (abbreviated as *M*) of the coating deposited at 80 mm was 8.9, which was the lowest of all the coatings studied. In addition, the 120-mm sprayed coating exhibited the highest Weibull modulus, 16.4, corresponding to the higher microstructure homogeneity compared with the other coatings.

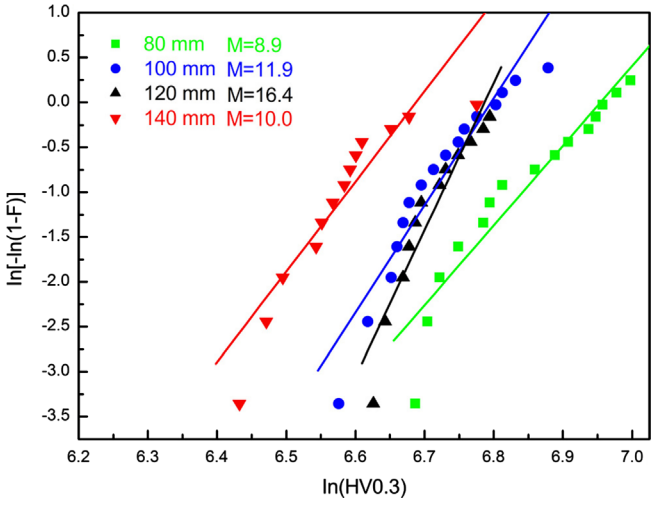

Fig. 2. Weibull modulus (*M*) of coatings deposited at different spray distances.

Xiong et al. [19] used a melting index (*MI*), defined as the ratio of the particle dwelling time to the time required to melt one in-flight particle, to indicate the molten state of a particle in the plasma jet. A higher *MI* indicated a better molten status. The *MI* can be expressed as follows:

$$MI = \frac{\Delta t_{fly}}{\Delta t_{melt}} = \frac{6k_l}{\rho L} \times \frac{1}{1+2/Bi} \times \frac{(T_f - T_m) \times \Delta t_{fly}}{r_p{}^2} \quad (1)$$

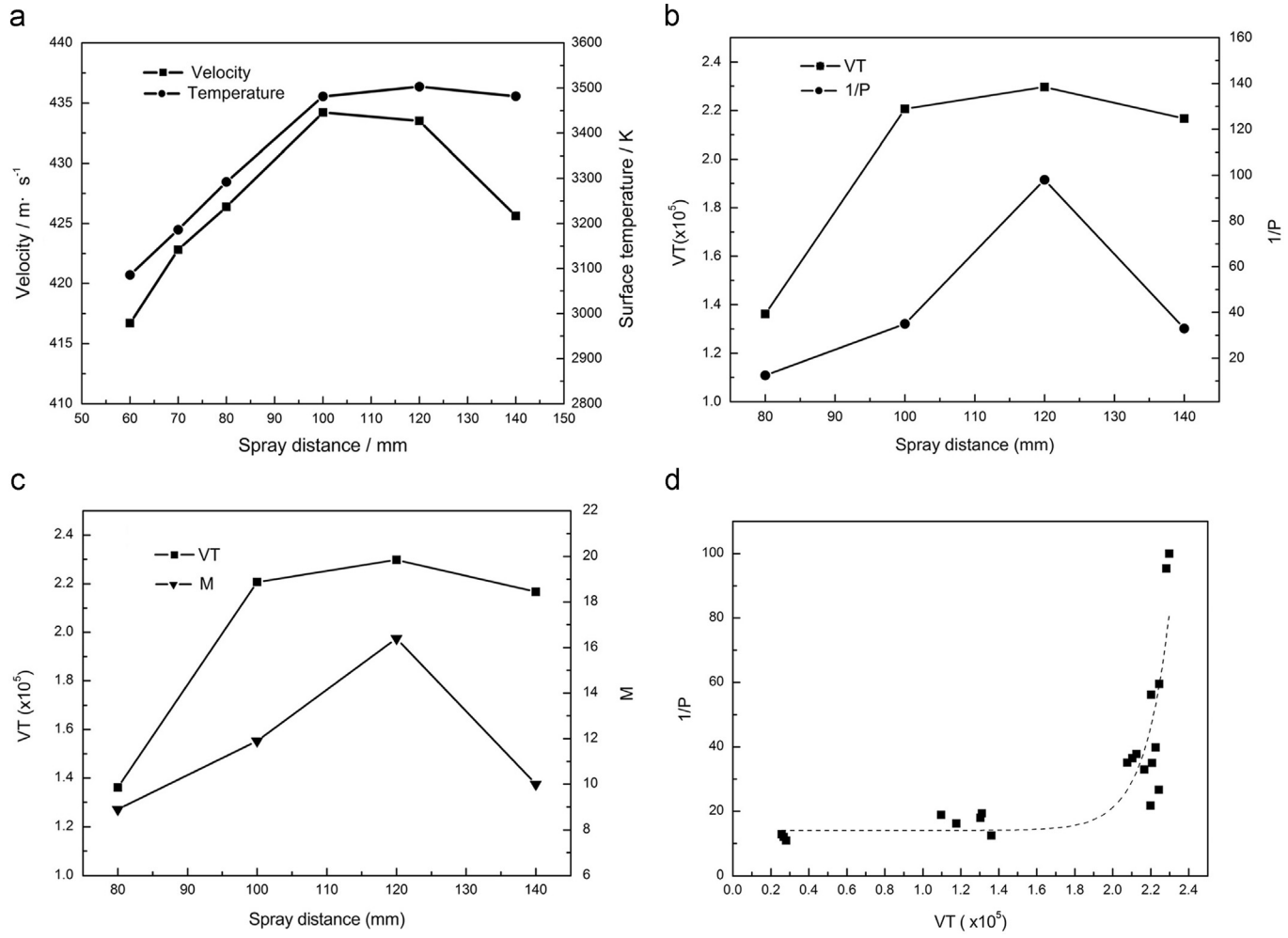

Fig. 3. Relationship between the in-flight property of particles and microstructure of as-sprayed coatings; (a) velocity and surface temperature at different spray distances; (b) *VT* and 1/*P* (reciprocal of porosity) versus spray distance; (c) *VT* and *M* (Weibull modulus) versus spray distance; and (d) 1/*P* as a function of *VT*.

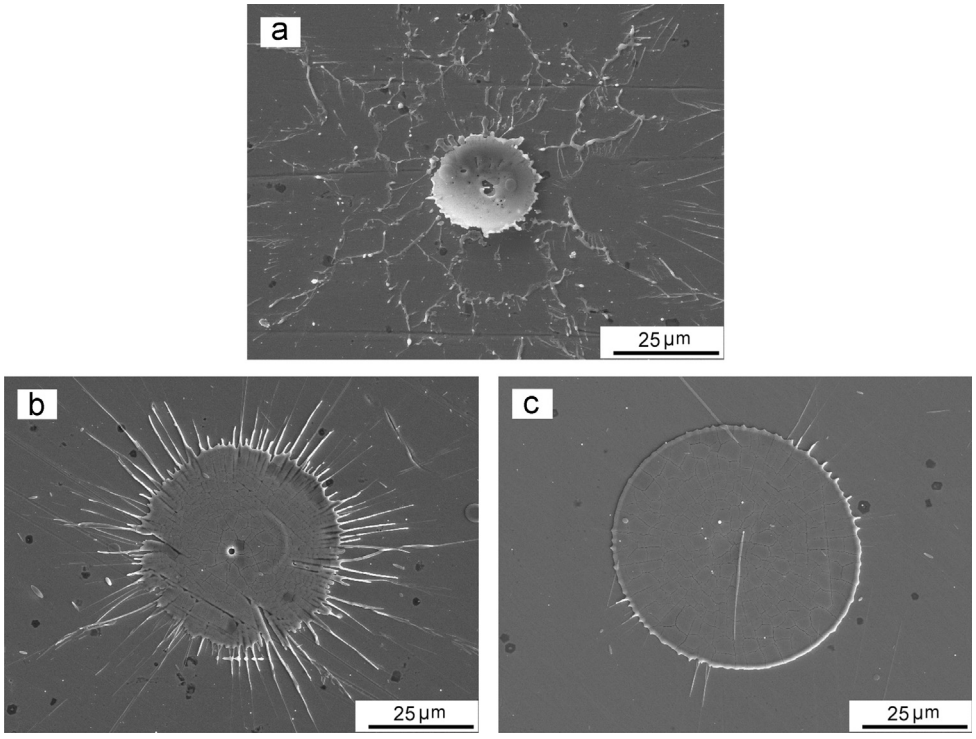

Fig. 4. Single flattened particles collected at different *VT* values: (a) 1.3×10^5, (b) 2.1×10^5, and (c) 2.3×10^5.

where *MI* is the melting index, Δt_{fly} is the particle dwell time in the plasma jet, Δt_{melt} is the complete melting time for one particle in the plasma jet, k_l is the thermal conductivity of a molten particle, T_f is the flame temperature, T_m is the particle melting point, ρ is the density of a particle, L is the latent heat of fusion, B_i is the Biot number, and r_p is the radius of a particle (assuming each particle is spherical).

Note that Δt_{fly} (dwell time) can be estimated as $2D/v$, where D is the spray distance and v is the particle velocity. Li et al. [20] indicated that an optimised spray distance in terms of the best melting state is determined by the position with the maximum *MI* value because the *MI* can be used as an indicator of the melting state. Thus, the following equation should be satisfied at the optimised spray distance:

$$\frac{d(MI)}{dD} = 0 \tag{2}$$

After performing some mathematical operations, the optimised spray distance D_{opt} can be expressed as follows [20]:

$$D_{opt} = \frac{\rho C_p}{6h} \times \frac{v d_p (T_s - T_m)}{T_s - T_g} \tag{3}$$

where D_{opt} is the optimised spray distance, C_p is the specific heat of the molten particle, d_p is the diameter of each particle, and T_g is the surrounding gas temperature near the substrate. Assuming d_p does not change during plasma spraying, from Eq. (3), D_{opt} is directly proportional to the value of $v(T_s - T_m)$. Therefore, a dimensionless quantity *VT* can be defined as:

$$VT = \frac{v(T_s - T_m)}{\beta} \tag{4}$$

where β is 1 m K s^{-1}, which makes the quantity *VT* dimensionless. The velocity (v) and surface temperature (T_s) were obtained by the Spray Watch 2i system. YSZ has a T_m of approximately 2973 K [21]. Fig. 3 shows the relationship between the in-flight properties of the particles and the microstructure of the resulting as-sprayed coatings. As shown in Fig. 3(a), the velocity of the in-flight particles attained a maximum value of 434 m s^{-1} at 100 mm, and the surface temperature of the in-flight particles attained a maximum value of 3503 K at 120 mm. For distances over 120 mm, the velocity of the in-flight particles dramatically decreased. In addition, as seen from Fig. 3(b and c), the *VT* value exhibited the same tendency as a function of the reciprocal of the porosity (1/*P*) and as a function of the Weibull modulus (*M*) as the coatings for different spray distances did. At the spray distance of 120 mm, the *VT* value reached its maximum value, which corresponded to the greatest value for the reciprocal of the porosity and the highest Weibull modulus of the coatings. The above result indicated that the *VT* value can be used as feedback for controlling the microstructure of the as-sprayed coatings. In addition, a different *VT* value was designed by adjusting the spray parameters (not shown in this work). The result of designing a different *VT* value is shown in Fig. 3(d), where the reciprocal of the porosity exhibited an exponential relationship with the *VT* value. When the *VT* value reached approximately 2.3×10^5, the value of the reciprocal of the porosity significantly increased. The morphology, shape, spreading and solidification behaviour of the single splats are known to substantially influence the characteristics of the final as-sprayed coatings. In this study, a single splat was deposited onto a mirror-polished GH3030 nickel-based superalloy substrate by placing a V-shaped shield with a 1-mm diameter hole (through which particles could pass) in front of the substrate during spray

coating. Fig. 4 shows the morphology of a single splat, i.e., a single in-flight particle impacted upon the polished substrate. As shown in Fig. 4(a), the single splat collected at the *VT* value of 1.3×10^5 almost completely disintegrated, and only a central solidified core remained on the substrate surface. As the *VT* value increased, as seen from Fig. 4(b and c), the splat morphology changed from splash-like to disk-shaped when the *VT* value was approximately 2.3×10^5. Compared with the splash-like splats, the disk-shaped splats could increase the effective bonding surface between the splats, thereby leading to the decrease of the inter-splat pores. Therefore, when the *VT* value was approximately 2.3×10^5, the value of the reciprocal of the porosity significantly increased, which corresponded with the results shown in Fig. 3(d). This *VT* value was defined as the "transition *VT* value". Note that the substrate was controlled to a level of 150 ± 30 °C during the process of coating deposition and splat collection. Thus, the effect of the substrate temperature on the morphology of the single splats was not discussed in this study.

4. Conclusions

In this study, yttria-stabilised zirconia (YSZ) coatings were deposited by a high-efficiency supersonic atmospheric plasma spraying (SAPS) system. The effect of the in-flight properties of the sprayed particles on the microstructure of the resulting coatings was studied. The *VT* value, defined as a function of velocity and surface temperature of the in-flight particles, was observed to be directly proportional to the reciprocal of the porosity and to the structural uniformity of the coatings. When the *VT* value was 2.3×10^5 (considered the transition *VT* value for the coatings studied), the porosity of the SAPS-coatings was significantly reduced. Thus, the *VT* value can be used as a simple indicator for tailoring the microstructure of SAPS-coatings.

Acknowledgements

This work was supported by the National Basic Research Program (Grant no. 2013CB035701), the National Natural Science Foundation for the Youth of China (Grant no. 51202187) and the Research Fund of the Key Laboratory for Advanced Technology in Environmental Protection of Jiangsu Province (Grant no. AE201006).

References

[1] A.G. Evans, D.R. Mumm, J.W. Hutchinson, G.H. Meier, F.S. Pettit, Mechanisms controlling the durability of thermal barrier coatings, Progress in Materials Science 46 (2001) 505–553.
[2] G.D. Girolamo, F. Marra, C. Blasi, E. Serra, T. Valente, Microstructure, mechanical properties and thermal shock resistance of plasma sprayed nanostructured zirconia coatings, Ceramics International 37 (2011) 2711–2717.
[3] S. Fantassi, M. Vardelle, A. Vardelle, P. Fauchais, Influence of the velocity of plasma-sprayed particles on splat formation, Journal of Thermal Spray Technology 2 (1993) 379–384.
[4] H. Liu, E. Lavernia, R. Rangel, Numerical simulation of impingement of molten Ti, Ni, and W droplets on a flat substrate, Journal of Thermal Spray Technology 2 (1993) 369–378.
[5] M. Bertagnolli, M. Marchese, G. Jacucci, Modeling of particles impacting on a rigid substrate under plasma spraying conditions, Journal of Thermal Spray Technology 4 (1995) 41–49.
[6] H. Fujimoto, Y. Shiotani, A.Y. Tong, T. Hama, H. Takuda, Three-dimensional numerical analysis of the deformation behavior of droplets impinging onto a solid substrate, International Journal of Heat and Fluid Flow 33 (2007) 317–332.
[7] M. Vardelle, A. Vardelle, A. Leger, P. Fauchais, D. Gobin, Influence of particle parameters at impact on splat formation and solidification in plasma spraying processes, Journal of Thermal Spray Technology 4 (1995) 50–58.
[8] J. Mostaghimi, M. Pasandideh-Fard, S. Chandra, Dynamics of splat formation in plasma spray coating process, Plasma Chemistry and Plasma Processing 22 (2002) 59–84.
[9] A. Vardelle, M. Vardelle, P. Fauchais, Influence of velocity and surface temperature of alumina particles on the properties of plasma sprayed coatings, Plasma Chemistry and Plasma Processing 2 (1982) 255–291.
[10] M. Friis, C. Persson, J. Wigren, Influence of particle in-flight characteristics on the microstructure of atmospheric plasma sprayed yttria stabilized ZrO_2, Surface and Coatings Technology 141 (2001) 115–127.
[11] P. Nylé, A. Hansbo, M. Friis, L. Pejryd, Investigation of particle in-flight characteristics during atmospheric plasma spraying of yttria stabilized ZrO_2: Part 2. Modeling, Journal of Thermal Spray Technology 10 (2001) 359–366.
[12] J. Cizek, K.A. Khor, Role of in-flight temperature and velocity of powder particles on plasma sprayed hydroxyapatite coating characteristics, Surface and Coatings Technology 206 (2012) 2181–2191.
[13] Z. Han, B. Xu, H. Wang, S. Zhou, A comparison of thermal shock behavior between currently plasma spray and supersonic plasma spray CeO_2–Y_2O_3–ZrO_2 graded thermal barrier coatings, Surface and Coatings Technology 201 (2007) 5253–5256.
[14] X.C. Zhang, B.S. Xu, S.T. Tu, F.Z. Xuan, H.D. Wang, Y.X. Wu, Effect of spraying power on the microstructure and mechanical properties of supersonic plasma-sprayed Ni-based alloy coatings, Applied Surface Science 254 (2008) 6318–6326.
[15] X.C. Zhang, B.S. Xu, Y.X. Wu, F.Z. Xuan, S.T. Tu, Porosity, mechanical properties, residual stresses of supersonic plasma-sprayed Ni-based alloy coatings prepared at different powder feed rates, Applied Surface Science 254 (2008) 3879–3889.
[16] Y. Bai, Z.H. Han, H.Q. Li, C. Xu, Y.L. Xu, C.H. Ding, J.F. Yang, Structure–property differences between supersonic and conventional atmospheric plasma sprayed zirconia thermal barrier coatings, Surface and Coatings Technology 205 (2011) 3833–3839.
[17] H. Zhou, F. Li, B. He, J. Wang, B.-d. Sun, Air plasma sprayed thermal barrier coatings on titanium alloy substrates, Surface and Coatings Technology 201 (2007) 7360–7367.
[18] A. Dey, A.K. Mukhopadhyay, S. Gangadharan, M.K. Sinha, D. Basu, N.R. Bandyopadhyay, Nanoindentation study of microplasma sprayed hydroxyapatite coating, Ceramics International 35 (2009) 2295–2304.
[19] H.B. Xiong, L.L. Zheng, L. Li, A. Vaidya, Melting and oxidation behavior of in-flight particles in plasma spray process, International Journal of Heat and Mass Transfer 48 (2005) 5121–5133.
[20] L. Li, A. Vaidya, S. Sampath, H.B. Xiong, L. Zheng, Particle characterization and splat formation of plasma sprayed zirconia, Journal of Thermal Spray Technology 15 (2006) 97–105.
[21] R. Dhiman, A.G. McDonald, S. Chandra, Predicting splat morphology in a thermal spray process, Surface and Coatings Technology 201 (2007) 7789–7801.